



Iranian Research Organization
for Science and Technology
(IROST)

Advances
Environmental
Technology



Journal home page: <https://aet.irost.ir/>

Effect of mass transport limitation and pyrite particulate on the continuous electro-Fenton process treatment of textile industrial dye

Imran Ahmad^{1*}, Debolina Basu¹

¹ Civil Engineering Department, Motilal Nehru National Institute of Technology, Allahabad, India

ARTICLE INFO

Document Type:
Research Paper

Article history:
Received 8 March 2022
Received in revised form
31 October 2022
Accepted 1 November 2022

Keywords:
Reactive orange 16
Continuous electro-Fenton
process
Mass transport
Pyrite particulate electrode

ABSTRACT

The current study focused on the charge and mass transport effect on the continuous electro-Fenton (EF) process treatment of synthetic Reactive orange 16 (RO16) dye using low-cost stainless-steel electrodes and sodium chloride (NaCl) supporting electrolytes, respectively. Lab-scale experiments were carried out in a 500 mL volume reactor cell at various initial RO16 dye concentrations (75-250 mg/L) and flow rates (0.05-0.4 L/h). The results showed that the decolorization rate increased quantitatively with an increment of the RO16 dye concentration and flow rate due to the mass transport limitation. Increasing the mass flow rate increased the mass transfer coefficient (k_m), improving the kinetics of the decay. It was found that regardless of inflow concentrations, the dye removal efficiency increased with the flow rate. Additionally, the degradation rate, elimination capacity, current efficiency (CE), and specific energy requirement were estimated for the process. A dimensionless current density relation was generated for the developed continuous stirred tank to describe the kinetics and mass transfer relationship towards the overall reaction rate contribution. It was found that the stainless-steel anode electrode proved to be preferable due to lower energy consumption (6.5 kWh m^{-3}) and less iron sludge production. Additionally, the application of pyrite (FeS_2) particulate electrode increased the process efficiency ($\sim 5\%$) for TOC removal and current mineralization while maintaining its sustainability for reuse.

1. Introduction

In the current era, overexploitation of natural resources caused by urbanization, industrialization, and rapid population growth has endangered the naturally balanced ecological system [1]. It has exacerbated many environmental

problems, among which environmental pollution and depletion of potable water are very serious. Industrialization has caused an enormous increase in global water demand. The incapability of water substitution for huge industrial applications has resulted in a water crisis. The UN-World Water Development reported that around 3.5 to 4.5 billion

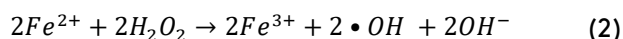
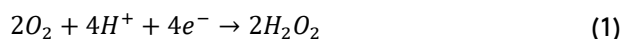
*Corresponding author:

Email: imran@mnnit.ac.in

DOI:10.22104/AET.2022.5547.1502

people might face severe water problems in the coming three decades if the water crisis is sustained. Worldwide water stress in terms of quality has also emerged as a result of a failure to adopt strict rules for industrial water treatment and a lack of effective technologies. The textile industry uses huge quantities of water and chemicals for the wet processing of materials and releases an enormous quantity of polluted effluent into the environment [2]. This adversely affects human health and aquatic life [3]. The aromatic amine group of dyes effluent inflicts significant damage because of its poisonous nature and biological degradation resistivity [4]. A genotoxic study confirmed the carcinogenic nature of azo dyes, which is also responsible for allergic contact dermatitis and respiratory illness [5,6]. The textile industry has often employed these dyes for coloring purposes because of their lower price and excellent chromophore characteristics. In the last few decades, an extensive number of industrial effluent treatment technologies, including physical [7], chemical [8], biological [9], and advanced oxidation processes [10], have been widely tested and documented in the literature. Despite several research publications on textile dye decolorization, the vast majority of laboratory-developed setups failed when they were scaled up or tested with real industrial wastewater. The possible reasons could be (i) the complexity of the industrial mixture that comprised of different classes of dyes, including mono-azo, di-azo, poly-azo, reactive, acid, basic, etc.; (ii) alkalinity of the industrial effluent; (iii) high quantity of salt; and (iv) high treatment capacity requirement, i.e., the huge volume of wastewater treatment in a shorter period of time. Due to these reasons, developing an efficient, cost-effective, and practicably applicable technology continues to be challenging. Adopting a streamlined strategy for treating dye effluent with chemical engineering technology tools and methods throughout the process development is needed. Electrochemical methods have attracted the interest of environmental researchers to treat the different micro and macro pollutants from various industrial sectors, particularly from the textile industry [11]. The EF process is more commonly used than other electrochemical processes because of its high mineralization

efficiency, absence of harmful chemical additions, and environmental compatibility. In this process, hydrogen peroxide (H_2O_2) is produced in situ by reducing oxygen (O_2) on the cathode (Eq. 1), and the Fenton reaction occurs in the bulk solution under ferrous ions (Fe^{2+}) presentation (Eq. 2) [12–14]:

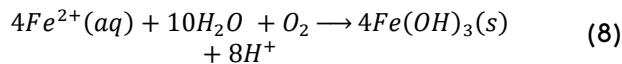
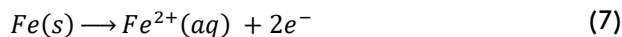
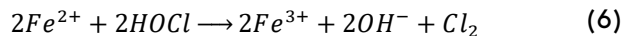
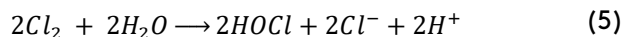


This technology proved to be more efficient and powerful because of the controlled and in situ H_2O_2 production, continuous hydroxyl radicals ($\bullet OH$) generation, and electro-regeneration of the Fe^{2+} through the cathodic reduction of Fe^{3+} (Eq. 3), which also reduced the production of iron sludge.

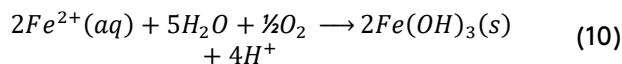
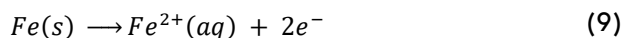


The two main categories of electrochemical oxidation are (i) direct and (ii) indirect. In the direct method of electrolysis, direct electron exchange with pollutants occurs at the anodic surface, destabilizing or degrading the pollutants, whereas, in the indirect electrolysis method, electron exchange with pollutants is mediated by active species. In both types of electrolysis, the redox catalysis chain connects anodic surfaces to contaminants via a series of reversibly or irreversibly generated electroactive compounds [15]. Physically absorbed hydroxyl radicals ($\bullet OH$) generated through non-active anodes also enhance the process efficiency by indirectly oxidizing the majority of organic molecules [16]. Due to this reason, several research papers suggest the application of the indirect oxidation approach for dye removal [11]. However, costly boron-doped diamond (BDD) electrode material has to be used for long-term practical applicability purposes in indirect oxidation [17]. It is also interesting that in the case of only using an active anode, i.e., without $\bullet OH$ radical availability for indirect oxidation, the occurrence of electrochemical degradation is still there because of a dissociation chemisorption reaction coupled with electron transfer [18]. The effectiveness of direct anodic oxidation is improved by the inclusion of many functional groups (e.g., azo linkages) on the dye molecules, making them electroactive for direct electron transfer [19]. Furthermore, the application of an active anode, e.g., stainless steel (or Fe electrode), proved to be

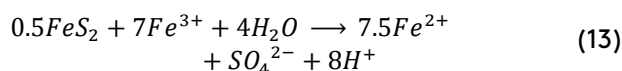
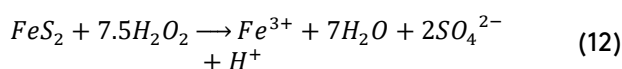
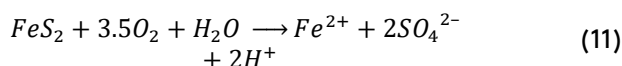
a viable solution for textile dye treatment due to its cost-effectivity, eco-friendly nature, and production of less sludge [20]. Employing a low-cost iron-based sacrificial anode also favored the electrocoagulation process that proved to be supportive for dye treatment (Eqs. 4 and 5) [21]. Therefore, a synergy, by using an active anode that might serve as a sacrificial anode along with a source of direct electro-oxidation, could be fascinating for electrochemical process improvement [21]. Additionally, using sodium chloride (NaCl) as a supporting electrolyte favored the mediated oxidation phenomenon (Cl_2 , HOCl) and electrocoagulation because of active chlorine generation and the availability of the iron-based anode (Eqs. 6 to 8) [22].



As dye effluents contain many chloride materials, this combined treatment (electrochemical cum electrocoagulation) will certainly favour the process [22]. The residual iron sludge formed at the stainless-steel anode during the electrocoagulation can be given as Eqs. 9 and 10 [21]:



Additionally, pyrite (FeS_2) crystal, a common iron ore, has successfully been tested as a substitute for the Fenton iron catalyst ($\text{Fe}^{2+}/\text{Fe}^{3+}$) [23]. The pyrite-added electro-Fenton process performed better than the classical electro-Fenton process as its presence regulated the iron ions in solution [24,25,26] (Eqs. 11 to 13). It also provided an acidic medium to the solution that was favourable for the process efficiency.



The current work focused on the charge and mass transport effect on the electro-Fenton process. The

continuous electro-Fenton process was studied with a combined effect of electrocoagulation by using stainless steel and sodium chloride (NaCl) as the working electrodes and supporting electrolyte, respectively. Reactive orange 16, the most common reactive dye used in the textile industry, was taken as a model pollutant. The lab-scale developed process was evaluated for degradation rate, elimination capacity, current efficiency, and specific energy requirement. A universal dimensionless current density parameter was also formulated for the employed study cell to evaluate better the competitiveness of charge transfer and mass transport. The effect on the mineralization efficiency of current with the pyrite particulate addition was also studied for the contentious EF process.

2. Material and methods

2.1. Experimental setup

For the experimental study, an undivided open cylindrical cell of borosilicate glass (500 mL volume) was used (Figure1).

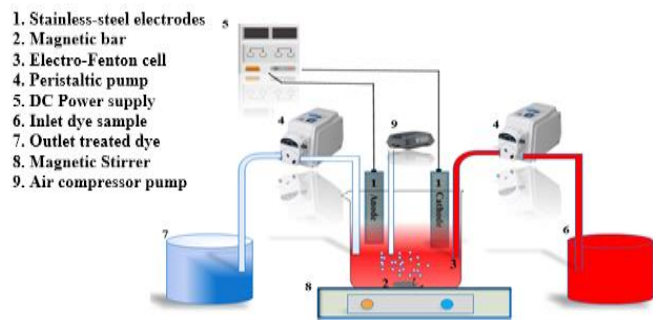


Fig. 1. Experimental lab setup of continuous electro-Fenton process.

The stainless steel (Kristeel brand) was used as the electrode plates for both the anode and cathode, with a total reactive submerged area of 20 cm^2 ($5 \text{ cm} \times 4 \text{ cm}$). An inter-electrode spacing of 2 cm was kept between the electrodes for all the experiments. A DC power source (Alpha 10A-50 V DC power supply) with an average applied current density of 35 mA/cm^2 was used as the external energy source. A magnetic stirrer (Remi) at 350 rpm and an air pump (Sobo, Model: SB333A, China) were used for stirring the aqueous solution and surging the atmospheric oxygen (1.5 L/min of flow rate) from the bottom of the reactor basin, respectively. The simulated dye solution was made

by dissolving and diluting the RO16 dye in distilled water to the desired concentration. Sodium chloride (NaCl) was used as a supportive electrolyte because of the chloride presentation in higher concentrations in most of the dye effluents [22]. For generated iron sludge separation, 10 min centrifugation action was done at a rate of 6000 rpm. All the tests were conducted at room temperature.

2.2. Chemicals used

The model dye RO16 was purchased from Sigma-Aldrich, India, and its characteristics are listed in Table 1. Other chemicals, such as NaCl, HCl, and NaOH, were purchased from Hi-Media Laboratories, India. 1N NaOH and 1N HCl were used for the solution pH adjustment. All the chemicals were of analytical grade (AR) and utilized in the same condition as supplied without additional purification.

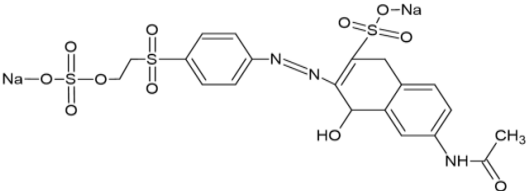
2.3. Characterization of pyrite crystals

The pyrite crystal (FeS₂) was arranged from Reiki Crystal Products (New Delhi, India) with a purity of

99.2%. First, it was milled and sieved for the particulate particles >80 nm. Then, to eliminate the surface impurities, the following process was adopted in a sequential manner:

5 min ultrasonication in 95% ethanol → 1.5 M Nitric Acid (HNO₃) wash → rinsing with deionized water → rinsing with 95% ethanol → final drying in a temperature controlled oven at 30°C. The scanning electron microscope (SEM) image of pyrite revealed its non-uniform nanoparticle shapes that ranged from 0.3 to 0.9 μm approximately (Figure 2a). In contrast, its X-ray diffraction (XRD) picture and the diffraction data files from the Joint Committee on Powder Diffraction Standards (JCPDS) (JADE 9, Materials Data Inc.) were in good agreement with each other (Figure 2b). In the aqueous solutions, the quantity of released Fe²⁺ ion from the pyrite dissolution was determined by spectrophotometry (UV-3000 LAB INDIA, Germany) using 1,10-phenantroline at a wavelength of 508 nm [27].

Table 1. Chemical structure and general characteristics of Reactive orange 16 dye.

Parameters	Reactive orange dye
Chemical formula	C ₂₀ H ₁₇ N ₃ Na ₂ O ₁₁ S ₃
Structure	
Molecular weight	697 g/mol
Maximum wavelength (λ _{max})	493 nm
Class of chromophore group	Mono-azo
Color index number	17757
Water solubility 19.85 °C (g/L)	>45
Acute oral toxicity (mg/kg)	2000
Fish toxicity (mg/l)	>490
pH (10 g/L H ₂ O)	6.2
COD (mg/g)	860

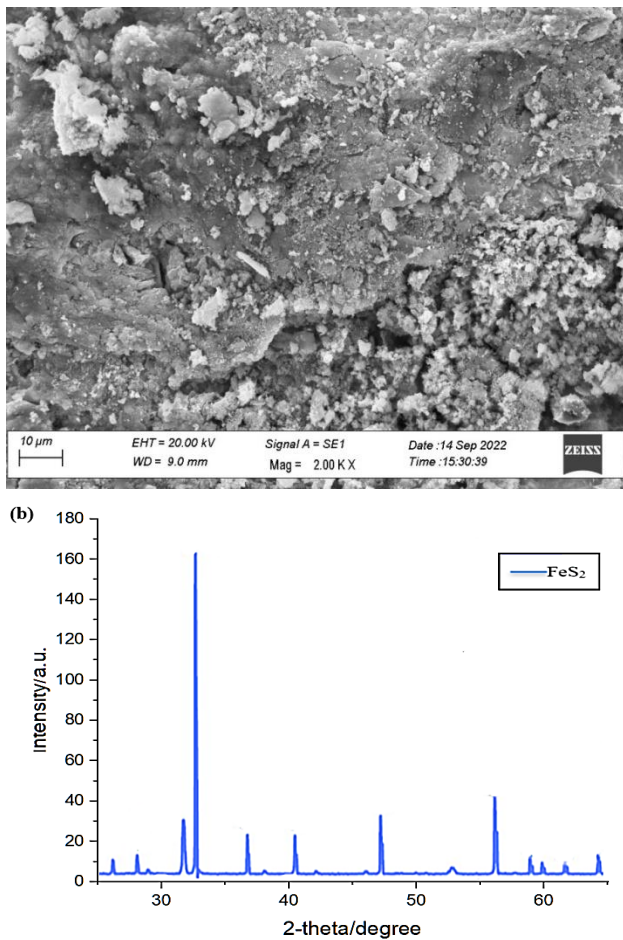


Fig. 2. SEM and XRD of the pyrite particulate.

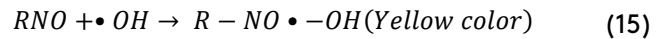
2.4. Analytical procedure

A Cyber Scan pH 1500 pH-meter from Eu-Tech Instruments (Singapore) was used to determine the pH of the solution. The change in absorbance was used to track the RO16 dye decolorization by using a UV-vis spectrophotometer (UV-3000 LAB INDIA, Germany) at λ_{max} . The percentage change of decolorization was computed by the following Eq. (14):

$$\text{Decolourization Rate (\%)} = \frac{C_o - C_t}{C_o} \times 100 \quad (14)$$

where C_o and C_t represent at initial and time t absorbance values, respectively. It should be emphasized that the concentration of $\bullet\text{OH}$ cannot be measured directly using chemical probes such as coumarin, but rather the amount of $\bullet\text{OH}$ produced or the cumulative concentration of products of the reaction with $\bullet\text{OH}$ can be estimated [14]. The fluorescence method was employed to quantify $\bullet\text{OH}$, using the N, N-dimethyl-p-nitroso-aniline (RNO) that acts as a spin trapper of $\bullet\text{OH}$ (Eq. 15). With the F97Pro fluorescence spectrophotometer

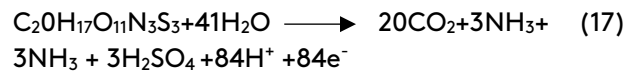
(Shanghai, China), the bleaching of the yellow color (RNO) was determined at 440 nm [28].



The quantity of $\bullet\text{OH}$ measured can be inferred indirectly by calculating the concentration of RNO. It should be noted that chemical probes cannot be used to test the concentration of $\bullet\text{OH}$ directly; instead, the volume of $\bullet\text{OH}$ produced or the total volume of products of the reaction with $\bullet\text{OH}$ can be estimated [29]. The mineralization efficiency (ME) of current I (A) in the electrolysis time period t_e (hr) was calculated by the following Eq. (16) [30,31]:

$$\text{ME (\%)} = \frac{100}{4.32 \times 10^7} \times \frac{n_e F V \Delta \text{TOC}}{m_c I t_e} \quad (16)$$

where F is the universal Faraday constant ($96,487 \text{ C mol}^{-1}$); V is the volume of the solution (L); ΔTOC is TOC decay of RO16 dye (mg/L); 4.32×10^7 is the factor of homogenized unit conversion; and m_c and n_e are the number of carbon atoms (20) and electrons (84) consumed per RO16 of the dye molecule, respectively (Eq. 17):



where D is a minimum distance from the epicenter of the flame to the object being considered and τ is the fraction of radiation heat transmitted through the atmosphere.

2.5. Degradation of RO16 dye in the continuous electro-Fenton process

The degradation of the RO16 dye was monitored for the continuous electro-Fenton process. The flow rate (varying from 0.05 to 0.4 L/h) of the synthetic dye solution was maintained with the help of a peristaltic pump. For constant reactor cell volume (500 mL) maintenance, the inflow and outflow rates were kept the same. The experiments were conducted at varying concentrations of dye (75, 100, 150, 200, and 250) with a constant electrolyte concentration of 0.4 M NaCl and pH 3.5. The continuous process was evaluated for elimination capacity (E_c) at various intake loading rates (Q) by using Eqs. (18) and (19).

$$E_c (\text{mg/Lh}) = \frac{(q_{in} - q_{out})Q_V}{V} \quad (18)$$

$$Q (\text{mg/Lh}) = \frac{q_{in}Q_V}{V} \quad (19)$$

where q_{in} and q_{out} are the inlet and outlet concentrations of dye; Q_v is the volumetric flow rate (L/h), and V is the constant volume of the reactor cell (L).

3. Results and discussion

3.1. Change in absorption spectra for RO16 dye characterization

In the preliminary study, the spectrophotometric approach was used to characterize and analyze the adequacy of the dye decolorization kinetics. A synthetic solution of 150 mg/L for RO16 dye was taken and treated electrochemically using the batch scale EF process. The change in the absorption spectra of RO16 dye is given in Figure 3 before (0th min) and after the 30th, 45th, and 60th min treatments. In the UV-Visible spectrophotometry analysis, the initial untreated RO16 dye displayed two strong peaks in the visible range at 493 nm and 398 nm and two peaks in the ultraviolet (UV) range at 256 nm and 299 nm. The peaks in visible ranges confirmed the aromatic structure of the dye, whereas the UV range peaks confirmed the conjugated structure of the azo bond (extended chromophores) [32]. The synthetic solution of dye that was subjected to the electrochemical treatment lost its color, as demonstrated by the disappearance of prominent peaks after 60 min of treatment without the emergence of any interference peaks that might be

caused by the matrix and intermediates created during the electrolysis process. This showed the reliability of the method for the continuous mode processes study because the absorbance measured at λ_{max} gives the maximum absorbance of the dye that was only linked with RO16 dye concentration, and this wavelength was not absorbed by any other species. Moreover, the loss of visible and UV range peaks confirmed the oxidation decomposition of the aromatic rings and its fragment breakdown in the dye molecule and intermediately generated products [33].

3.2. Continuous electro-Fenton process: Charge and mass transfer study

The performance of the continuous electro-Fenton process for RO16 dye treatment was studied at various concentrations (75-250 mg/L) and flow rates (0.05-0.4 L/h) (Table 2). The results for the decolorization efficiency and capacity of elimination are shown in Figure 4. The inlet loading rate (Q) was used to compute the reactor efficiency. For the dye concentrations 75 to 150 mg/L, the degradation rate showed a positive trend with the increment in Q . The degradation rate obtained for 150 mg/L of the synthetic dye solution with Q as 120 mg/(L h) was 76 mg/(L h) (~63 percent of removal efficiency for inlet Q) for a 30 min residence time. This was the maximum capacity of elimination for the RO16 dye.

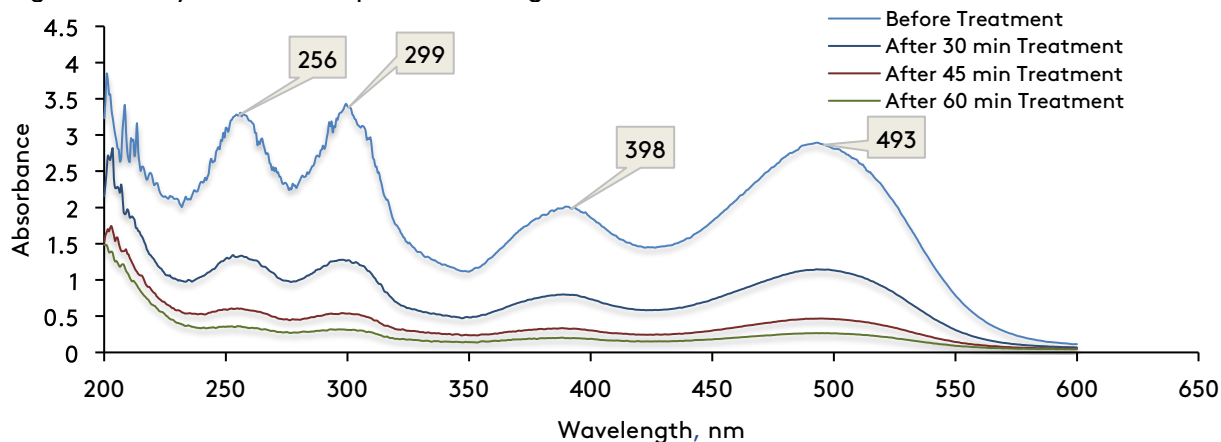
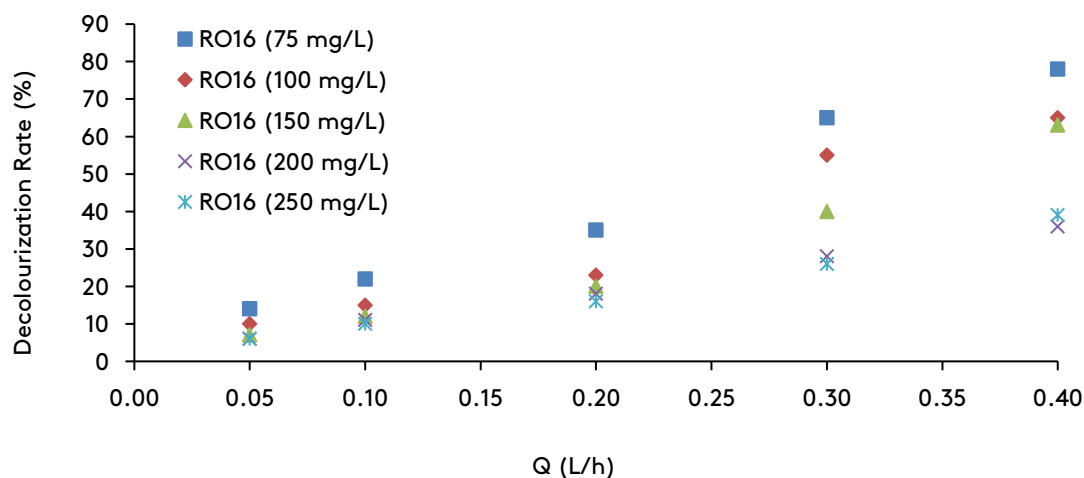


Fig. 3. Absorption spectrum of the RO16 for the electro-Fenton process treatment ($[RO16]_{initial} = 150$ mg/L, pH=3.5, $[NaCl] = 0.4$ M, $V = 13$ Volt).

Table 2. Input data and corresponding results for the continuous electro-Fenton treatment of RO16 dye.

RO16 conc.	Flow rate (Q)	Rate of inlet loading	Removal efficiency	Elimination capacity	Current Efficiency	Specific Energy
(mg/L)	(L/h)	(mg/(L h))	(%)	(mg/(L h))	(%)	(kWh g-dye ⁻¹)
75	0.05	11.23	14	2.25	0.38	1.31
	0.10	28.25	22	9.02	1.06	0.775
	0.20	59	35	20.05	2.96	0.24
	0.30	92.75	65	71.5	8.51	0.186
	0.40	125	78	107.75	12.86	0.047
100	0.05	16	10	2.11	0.32	2.72
	0.10	42	15	8.1	0.96	1.78
	0.20	87	23	19.5	2.9	0.95
	0.30	129	55	63	7.6	23.8
	0.40	171	65	102	12.4	0.135
150	0.05	28.35	7	1.82	0.23	2.62
	0.10	64.5	12	6.2	0.78	1.55
	0.20	129	20	19.1	2.81	0.48
	0.30	194	40	48.5	5.4	0.221
	0.40	255	63	91	11.63	0.095
200	0.05	35	6	1.63	0.18	5.32
	0.10	87	11	4.8	0.57	3.13
	0.20	171	18	18.9	2.76	0.98
	0.30	258	28	36	4.2	0.44
	0.40	342	36	81	10.63	0.21
250	0.05	36	6	1.35	0.047	1.67
	0.10	105.5	10	3.15	0.35	1.06
	0.20	177	16	18.25	2.59	0.45
	0.30	315	26	21.21	2.54	0.14
	0.40	422	39	79	9.12	0.09

**Fig. 4.** Study of inlet concentration and flow rate effect on RO16 dye the removal efficiency.

Furthermore, with an increment of the inlet concentration, the treatment efficiency of the electrochemical process was also enhanced. Therefore, it could be concluded that the decay kinetics of the RO16 dye was affected by the inflow

concentrations of the dye solution. Another intriguing observation is that regardless of inflow concentrations, the removal efficiency increased with flow rate, i.e., with a decrease in retention time. For further insight into the flow rate effect

on process efficiency, a comparison of the applied current density (J_A), i.e., 35 mA/cm² to the initial limiting current density values (J_L^0), i.e., the dimensionless current density (ρ), was calculated as per Eq. (20):

$$\rho = \frac{J_A}{J_L^0} \quad (20)$$

Furthermore, J_L^0 can also be written in terms of the Faraday constant (F), mass transfer coefficient (k_M), and influent COD (COD_{inlet}) using Eq. (21) [34]:

$$J_L^0 = 4Fk_M COD_{inlet} \quad (21)$$

From Eqs. (20) and (21), a new Eq. (22) for ρ can be re-written as:

$$\rho = \frac{J_A}{4Fk_M COD_{inlet}} \quad (22)$$

From Eq. (22), it is clear that the value of k_M must be known in order to calculate ρ . For this purpose, the dimensionless Sherwood (S_w) number, expressed in terms of k_M , the equivalent dia. (d_{eq}), and the diffusivity (D_{ff}), was used and is given by Eq. (23) [35]:

$$S_w = \frac{k_M d_{eq}}{D_{ff}} \quad (22)$$

The Sherwood number (S_w) number further can be expressed as the function of dimensionless Reynolds (R_y) and Schmidt (S_m) numbers (Eq. 24) [36], whereas S_m is given by Eq. (25) [24] and R_y for a stirred cell can be calculated from Eq. (26) [37]:

$$S_w = \rho R_y^x S_m^y \quad (24)$$

$$S_m = \frac{D_{ff}}{\nu} \quad (25)$$

$$R_y = \frac{d^2 N}{\nu} \quad (26)$$

where ν , d , and N are the kinematic viscosity of the fluid, stirrer dia., and rotation speed, respectively. From Eqs. (23) to (26), the new form of the equation for k_M expression can be written as Eq. (27):

$$k_M = \frac{\rho}{d_{eq}} D_{ff}^{1-y} \nu^{y-x} (d^2 N)^x \quad (27)$$

Finally, from Eq. (22) and Eq. (27), the general dimensionless expression for current density (ρ) in a stirred cell can be proposed by following Eq. (28):

$$\rho = \frac{J_A}{4Fk_M COD_{inlet}} \frac{d_{eq}}{A} D_{ff}^{B-1} \nu^{C-B} (d^2 N)^{-B} \quad (28)$$

In this work, the constants d_{eq} , d , D_{ff} , N , A , B , and C were taken as 10.5 cm, 2 cm, 10^{-9} m²/s [38], 100 rpm, 8.917×10^{-7} m² s⁻¹ at 25°C (Engineering Toolbox, 2004), 0.228 [39], 0.66 [39], respectively. From the selected constants, the k_M value of 1.7×10^{-6} m/s was

calculated for the study, which falls within the range of values reported in other studies for the stirred cell operation ($\sim 5.9 \times 10^{-6}$ m/s) [40,41,42]. By the values of COD_{inlet} (Table 3), ρ as the function of the dye and its initial concentrations was calculated and is shown in Figure 5. In every case, its values ranged between 28 and 83 and were always greater than 1, i.e., J_A was always greater than J_L^0 . Consequently, it can be inferred that for the treatment process, decay kinetics was primarily controlled by mass transport [34,43]. Therefore, increasing Q , i.e., mass flow rate, increased k_M , which ultimately improved the kinetics of the decay process (Figure 6). To further access the process efficiency, the CE for the continuous electrochemical process was estimated as per Eq. (29) [44]:

$$CE(\%) = 100 \times \frac{n_e F X Q_V}{A_{sub} J_A} \quad (29)$$

where A_{sub} is the submerged surface area of the electrode (20 cm²), X is the current conversion yield ($(q_{in} - q_{out}) / q_{in}$), and n_e represents the electrons required (84) for the RO16 breakout in carbon dioxide via electrochemical combustion (Eq. 17). For the continuous mode operation, the specific energy (E_{sp}) requirement was also estimated by using Eq. (30) [45]:

$$E_{sp} = \frac{E_{cell} I}{C_{in} X Q_V} \quad (30)$$

where E_{cell} represents the cell voltage (V). For both current the efficiency and specific energy, Fig. 6 was drawn as a function of Q and $[RO16]_{initial}$. At optimum condition, the energy requirement for full decolorization was about 6.5 kWh m⁻³ compared to the aluminium anode electrode, which was around 11 kWh m⁻³, as previously reported [21]. Thus, for electrochemical treatment of RO16 dye stainless steel anode proved to be more preferable than the aluminium anode.

Table 3. The COD_{inlet} values for various RO16 dye concentration.

S. No.	RO16 dye concentration (mg/L)	COD_{inlet} (mili-mol-O ₂ /L)
1.	75	2.74
2.	100	3.65
3.	150	5.48
4.	200	7.31
5.	250	9.14

energy requirement and (b) to remove RO16 dye. Furthermore, the increasing and decreasing values of CE and E_{sp} with inlet concentration and flow rate confirmed the kinetics dependency and mass transport control of the continuous process. Also, the quantity of higher iron sludge generation

(about 4.8 g/h) supports the role of the electrocoagulation mechanism which is even lower than the aluminium sacrificial anode (about 2.8 times less) at optimum conditions [21].

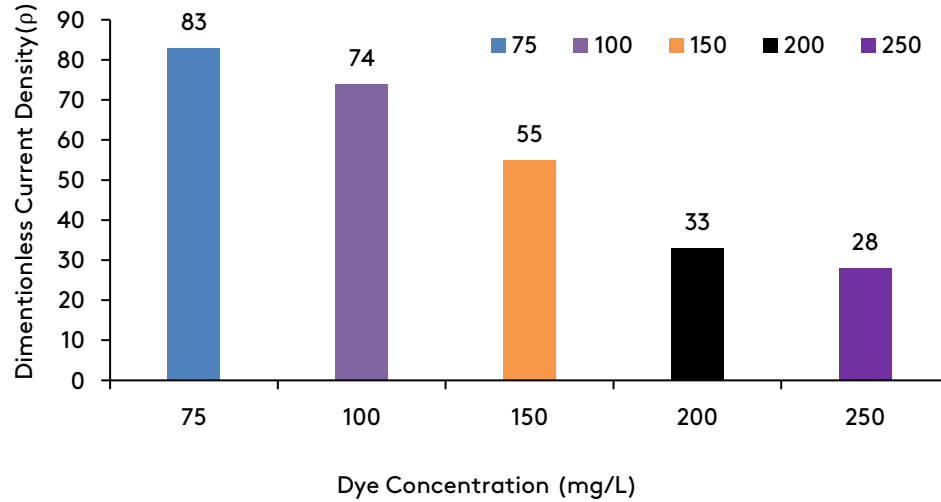


Fig. 5. Effect of inlet RO16 dye concentration (mg/L) on the dimensionless current density (ρ).

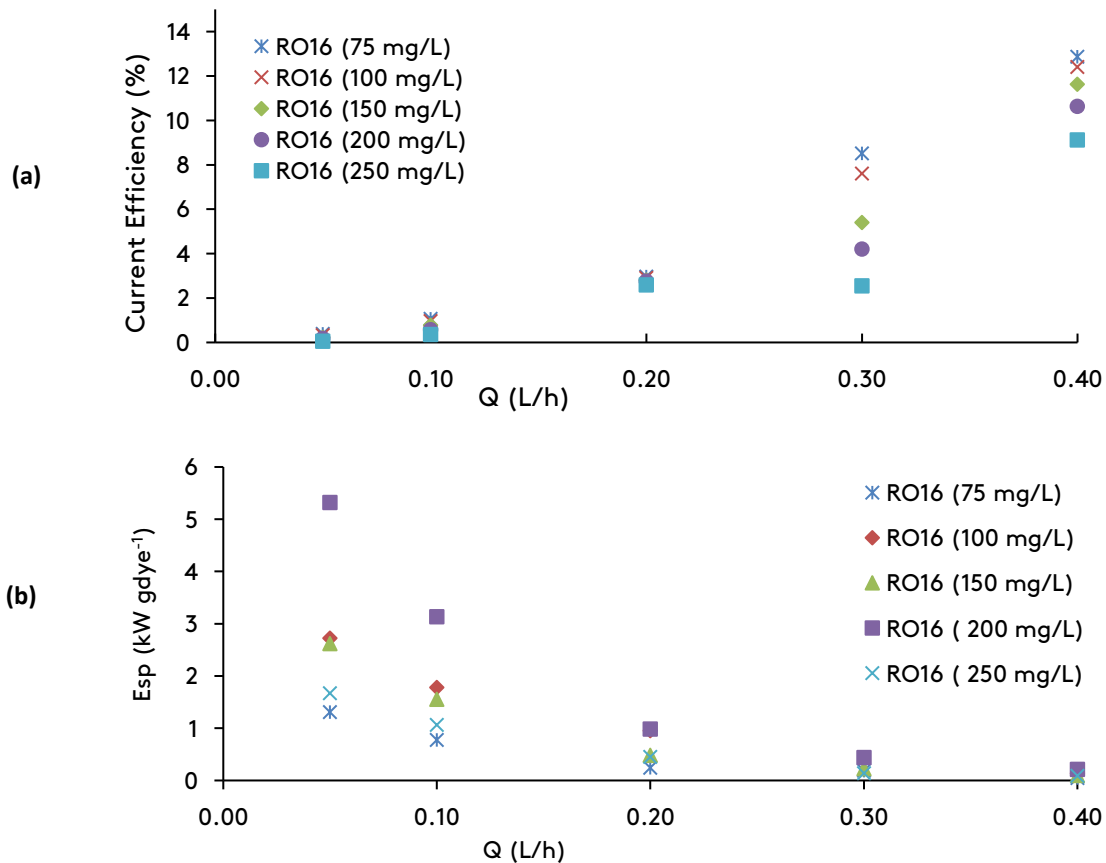


Fig. 6. Effect of flow rate and inlet concentration on the current efficiency: (a) the specific energy requirement and (b) to remove RO16 dye.

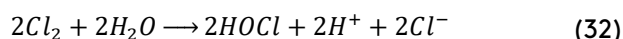
3.3. Role of supporting electrolyte NaCl

The chloride ion of the used supporting electrolyte NaCl produced *in-situ* hypochlorite that contributed to the oxidation process of the dye pollutants. For the confirmation of OCl^- role in the degradation kinetics of dye pollutants, the process was electrolyzed for 25 min with 0.25 M NaCl in the absence of the dye pollutant. The spectrum drawn through the UV-Vis Spectrophotometer showed peak absorption at 290 nm for OCl^- (Figure 7), which confirmed the presence of OCl^- in the electrochemical oxidation process. The following reactions are expected to occur in the process (Eqs. 31 to 34) [46]:

Anode: Main reaction:



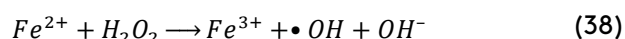
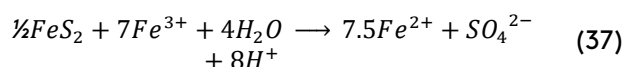
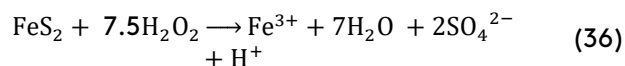
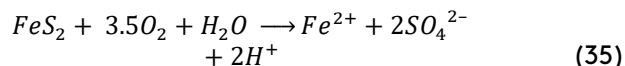
Bulk solution:



3.4. Role of pyrite particulate electrodes

The effect of the pyrite particulate electrode on the process was also carried out. For the unchanged experimental conditions (150 mL of RO16 dye solutions; 0.15 mM Fe^{2+} catalyst), both the traditional electro-Fenton process and the EF with pyrite particulate were tested. The results showed a higher mineralization rate for the pyrite particulate added electro-Fenton process. Total

TOC abatement that was about 75% in the traditional electro-Fenton process increased up to 80% with the pyrite added EF process at the end of the treatment (Figure 8a). This higher mineralization is attributed to the higher amount of Fe^{2+} ions generated from the pyrite particulate (3.5 mM for 2.5 g/L pyrites) with a self-regulating advantage at its surface (Eq. 35 to 37). The additionally generated Fe^{2+} ions favored the $\bullet\text{OH}$ production and process efficiency by the Fenton reaction, as explained in Eq. 38 [47,48,49].



The ME curve shown in Fig. 8b reveals that the pyrite particulate added electro-Fenton process resulted in greater process efficiency than the conventional electro-Fenton process (13.1 percent vs. 9.9 percent). These findings support pyrite as a potential particulate catalyst in the electrolysis treatment of persistent organic pollutants, such as azo dye, even when less active anodes such as stainless steel for the formation of $\text{M}(\bullet\text{OH})$ were used (M stands for metal electrode). During electrolysis, the drop in the ME confirmed the generation of more resistant intermediates and fewer organic products that accelerated the parasitic reactions (Eqs. 39 to 41).

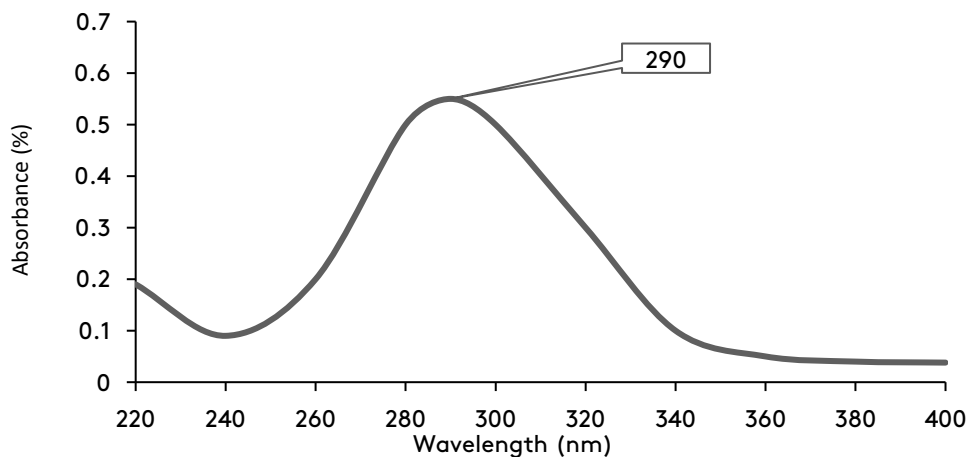
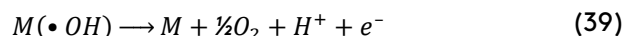
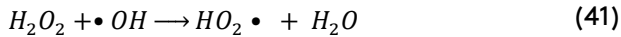


Fig. 7. UV-vis spectrum of OCl^- production from NaCl supporting electrolyte solution ($[\text{NaCl}] = 0.25\text{M}$; $t = 25$ min; $E = 12\text{V}$).





The result provides an economic benefit over the costlier price of the BDD electrode [50], as in the case of indirect oxidation of the electrochemical process for long-term applicability suitability. Additionally, at the end of every electrolysis process, the used pyrite can be re-collected, filtered, and reused, which is a considerable improvement in the sustainability of the process.

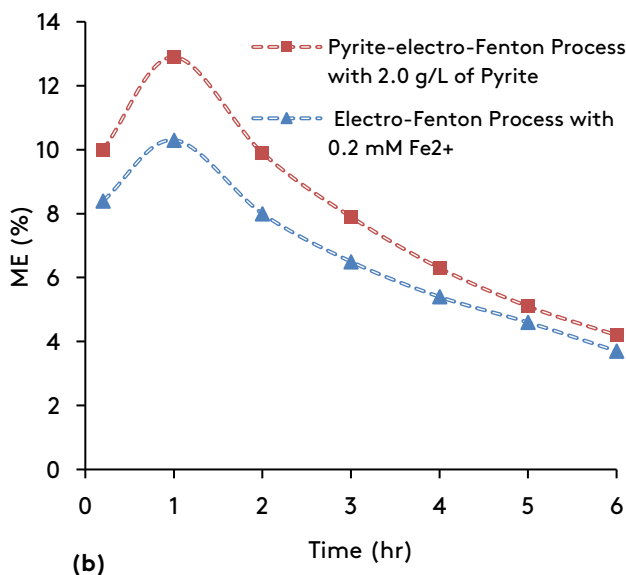
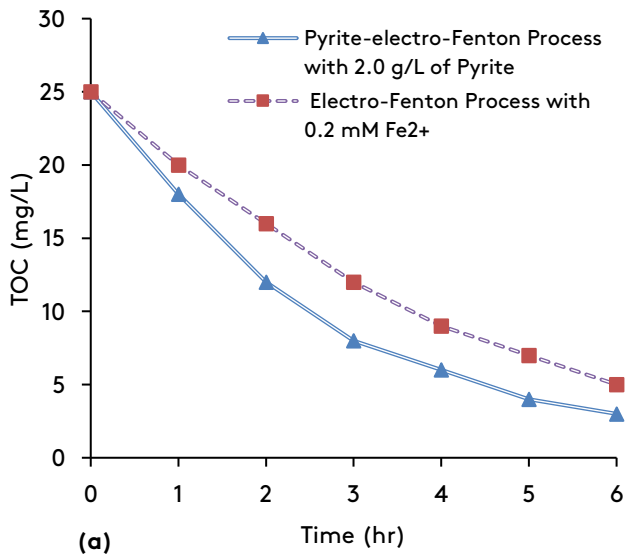


Fig. 8. (a) TOC removal vs. electrolysis time for the RO16 dye mineralization ($[RO16]_{initial}=150$ mL, $[NaCl]=0.05$ M, $pH=3$, $I=350$ mA; (b) Represent the corresponding ME curve.

4. Conclusions

In the current work, the continuous electro-Fenton process with stainless steel cost-effective electrodes and sodium chloride (NaCl) supporting electrolytes were used for the synthetic RO16 azo dye treatment. The result of the study shows that the decay kinetics of the RO16 dye was affected by the inflow concentrations of the dye solution and primarily controlled by mass transport. Increasing the mass flow rate increased the mass transfer coefficient (k_M) and so improved the kinetics of the decay. Also, regardless of inflow concentrations, the removal efficiency increased with the flow rate, i.e., a decrease in retention time. It was found that for the electrochemical treatment of RO16 dye, the stainless-steel anode electrode was preferred over the aluminium anode due to lower energy requirements (6.5 kWh m^{-3} vs. 11 kWh m^{-3}) and less iron sludge production (almost 2.8 times lower) [18]. The UV-Vis spectrophotometer results of the NaCl electrolyte confirmed the presence of OCl^- ions in the electrochemical oxidation process. Additionally, the applicability of pyrite particulate showed good improvement (~5%) in efficiency while maintaining its sustainability for reuse. Thus, the result showed an efficient and economical benefit over the costlier BDD electrode used in the case of indirect oxidation of the electrochemical process for long-term applicability.

Acknowledgment

The authors appreciate the Civil Engineering Department, Motilal Nehru National Institute of Technology Allahabad, for providing the laboratory facility.

References

- [1] Ruba, D. A. (2021). Modelling turbidity removal by poly-aluminium chloride coagulant using gene expression. *Advances in environmental technology*, 7(4), 263-273.
- [2] Hasanbeigi, A., Price, L. (2015). A technical review of emerging technologies for energy and water efficiency and pollution reduction in the textile industry. *Journal of cleaner production*, 95, 30-44.
- [3] Yousef, D., Bizhan H., Amin A., Moein N. (2021). Treatment of wastewater by a combined technique of adsorption, electrocoagulation

- followed by membrane separation. *Advances in environmental technology*, 7(3), 171-183.
- [4] Holkar, C. R., Jadhav, A. J., Pinjari, D. V., Mahamuni, N. M., Pandit, A. B. (2016). A critical review on textile wastewater treatments: Possible approaches. *Journal of Environmental. management.*, 182(532), 351-366.
- [5] Schneider, K., Hafner, C., Jäger, I. (2004). Mutagenicity of textile dye products. *Journal of Applied toxicology: An international journal*, 24(2), 83-91.
- [6] Gürses, A., Açıkyıldız, M., Güneş, K., Gürses, M. S. (2016). Dyes and pigments: Their structure and properties. Springer
- [7] Sharma, V., Shahnaz, T., Subbiah, S., Narayanasamy, S. (2020). New insights into the remediation of water pollutants using nanobentonite incorporated nanocellulose chitosan based aerogel. *Journal of polymers and the environment*, 28(7), 2008-2019.
- [8] Durai, N. J., Gopalakrishna, G. V. T., Padmanaban, V. C., Selvaraju, N. (2020). Oxidative removal of stabilized landfill leachate by Fenton's process: process modeling, optimization and analysis of degraded products. *RSC advances*, 10(7), 3916-3925.
- [9] Padmanaban, V. C., Geed, S. R. R., Achary, A., Singh, R. S. (2016). Kinetic studies on degradation of Reactive Red 120 dye in immobilized packed bed reactor by *Bacillus cohnii* RAPT1. *Bioresource technology*, 213, 39-43.
- [10] Aquino, J. M., Rocha-Filho, R. C., Rodrigo, M. A., Sáez, C., Cañizares, P. (2013). Electrochemical degradation of the Reactive Red 141 dye using a boron-doped diamond anode. *Water, air, and soil pollution*, 224(1), 1-10.
- [11] Martínez-Huitle, C. A., & Brillas, E. (2009). Decontamination of wastewaters containing synthetic organic dyes by electrochemical methods: a general review. *Applied catalysis B: Environmental*, 87(3-4), 105-145.
- [12] Brillas, E., Boye, B., Sirés, I., Garrido, J. A., Rodríguez, R. M., Arias, C., Cabot, P., Comninellis, C. (2004). Electrochemical destruction of chlorophenoxy herbicides by anodic oxidation and electro-Fenton using a boron-doped diamond electrode. *Electrochimica acta.*, 49(25), 4487-4496.
- [13] Sirés, I., Oturan, N., Oturan, M. A., Rodríguez, R. M., Garrido, J. A., Brillas, E. (2007). Electro-Fenton degradation of antimicrobials triclosan and triclocarban. *Electrochimica. Acta.*, 52(17), 5493-5503.
- [14] Zhou, M. H., Yu, Q. H., Lei, L. C. (2008). The preparation and characterization of a graphite PTFE cathode system for the decolorization of C.I. Acid Red 2. *Dyes and Pigment*, 77(1), 129-136.
- [15] Panizza, M., Cerisola, G. (2009). Direct and mediated anodic oxidation of organic pollutants. *Chemical reviews*, 109(12), 6541-6569.
- [16] Mousset, E., Wang, Z., Olvera-Vargas, H., Lefebvre, O. (2018). Advanced electrocatalytic pre-treatment to improve the biodegradability of real wastewater from the electronics industry- A detailed investigation study. *Journal of hazardous materials*, 360, 552-559.
- [17] Nidheesh, P. V., Divyapriya, G., Oturan, N., Trelu, C., Oturan, M. A. (2019). Environmental applications of boron-doped diamond electrodes: 1. Applications in water and wastewater treatment. *ChemElectroChem*, 6(8), 2124-2142.
- [18] Mohan, N., Balasubramanian, N., Basha, C. A. (2007). Electrochemical oxidation of textile wastewater and its reuse. *Journal of hazardous materials*, 147, 644-651.
- [19] Michaelis, L. (1935). Semiquinones, the Intermediate Steps of Reversible Organic Oxidation-Reduction. *Chemical reviews*, 16(2), 243-286.
- [20] Bassyouni, D. G., Hamad, H. A., El-ashtouky, E. Z., Amin, N. K., El-latif, M. M. A. (2017). Comparative performance of anodic oxidation and electrocoagulation as clean processes for electrocatalytic degradation of diazo dye Acid Brown 14 in aqueous medium. *Journal of hazardous materials*, 335, 178-187.
- [21] Arslan-Alaton, I., Kabdaşlı, I., Hanbaba, D., Kuybu, E. (2008). Electrocoagulation of a real reactive dyebath effluent using aluminum and stainless-steel electrodes. *Journal of hazardous materials*, 150, 166-173.

- [22] Hakizimana, J. N., Gourich, B., Chafi, M., Stiriba, Y., Vial, C., Drogui, P., Naja, J. (2017). Electrocoagulation process in water treatment: A review of electrocoagulation modeling approaches. *Desalination*, *404*, 1-21.
- [23] Holmes, P. R., Crundwell, F. K. (2000). The kinetics of the oxidation of pyrite by ferric ions and dissolved oxygen: an electrochemical study. *Geochimica et cosmochimica acta*, *64*(2), 263-274.
- [24] Bae, S., Kim, D., Lee, W. (2013). Degradation of diclofenac by pyrite catalyzed Fenton oxidation. *Applied catalysis B: Environmental*, *134*, 93-102.
- [25] Choi, K., Bae, S., Lee, W. (2014a). Degradation of off-gas toluene in continuous pyrite Fenton system. *Journal of hazardous materials*, *280*, 31-7.
- [26] Choi, K., Bae, S., Lee, W. (2014). Degradation of pyrene in cetylpyridinium chloride-aided soil washing wastewater by pyrite Fenton reaction. *Chemical engineering journal*, *249*, 34-41.
- [27] Furman, N.H., 1975. Standard Methods of Chemical Analysis, sixth. ed., R. E. Krieger Pub. Co., New York.
- [28] Comninellis, C. (1994). Electrocatalysis in the electrochemical conversion/combustion of organic pollutants for waste water treatment. *Electrochimica. acta.*, *39*(11-12), 1857-1862.
- [29] Kubo, D., Kawase, Y. (2018). Hydroxyl radical generation in electro-Fenton process with in situ electro-chemical production of Fenton reagents by gas-diffusion-electrode cathode and sacrificial iron anode. *Journal of cleaner production*, *203*, 685-695.
- [30] Brillas, E., Sirés, I., Oturan, M. A. (2009). Electro-Fenton process and related electrochemical technologies based on Fenton's reaction chemistry. *Chemical reviews*, *109*, 6570-6631.
- [31] Garcia-Segura, S., Garrido, J. A., Rodríguez, R. M., Cabot, P. L., Centellas, F., Arias, C., Brillas, E. (2012). Mineralization of flumequine in acidic medium by electro-Fenton and photoelectro-Fenton processes. *Water research*, *46*(7), 2067-2076.
- [32] Padmanaban, V. C., Selvaraju, N., Vasudevan, V. N., Achary, A. (2018). Augmented radiolytic ($^{60}\text{Co } \gamma$) degradation of direct red 80 (Polyazo dye): optimization, reaction kinetics and G-value interpretation. *Reaction kinetics, mechanisms and catalysis*, *125*(1), 433-447.
- [33] Wu, J., Gao, H., Yao, S., Chen, L., Gao, Y., Zhang, H. (2015). Degradation of Crystal Violet by catalytic ozonation using Fe/activated carbon catalyst. *Separation and purification technology.*, *147*, 179-185.
- [34] Panizza, M., Michaud, P. A., Cerisola, G., Comninellis, C. (2001). Anodic oxidation of 2-naphthol at boron-doped diamond electrodes. *Journal of electro analytical chemistry*, *507*(1-2), 206-214.
- [35] Cañizares, P., García-Gómez, J., Fernández de Marcos, I., Rodrigo, M. A., Lobato, J. (2006). Measurement of mass-transfer coefficients by an electrochemical technique. *Journal of chemical education*, *83*(8), 1204.
- [36] Anglada, Á., Urtiaga, A. M., Ortiz, I. (2010). Laboratory and pilot plant scale study on the electrochemical oxidation of landfill leachate. *Journal of hazardous materials*, *181*(1-3), 729-735.
- [37] Fitschen, J., Maly, M., Rosseburg, A., Wutz, J., Wucherpfennig, T., Schlüter, M. (2019). Influence of spacing of multiple impellers on power input in an industrial-scale aerated stirred tank reactor. *Chemie-ingenieur-technik*, *91*, 1794-1801.
- [38] Scialdone, O., Galia, A., Randazzo, S. (2012). Electrochemical treatment of aqueous solutions containing one or many organic pollutants at boron doped diamond anodes. Theoretical modeling and experimental data. *Chemical engineering journal*, *183*, 124-134.
- [39] Selman, J. R., Tobias, C. W. (1978). Mass-transfer measurements by the limiting-current technique. In *advances in chemical engineering* (Vol. 10, pp. 211-318). Academic press.
- [40] Dos Santos, E. V., Sena, S. F. M., da Silva, D. R., Ferro, S., De Battisti, A., Martínez-Huitle, C. A. (2014). Scale-up of electrochemical oxidation system for treatment of produced water generated by Brazilian petrochemical industry. *Environmental science and pollution research*, *21*(14), 8466-8475.
- [41] Mousset, E., Puce, M., Pons, M. N. (2019b). Advanced electro-oxidation with boron-doped

- diamond for acetaminophen removal from real wastewater in a microfluidic reactor-Kinetics and mass transfer studies. *Chem Electro Chem*, 6, 2908-2916.
- [42] Rocha, J. H. B., Solano, A. M. S., Fernandes, N. S., da Silva, D. R., Peralta-Hernandez, J. M., Martínez-Huitle, C. A. (2012). Electrochemical degradation of remazol red BR and novacron blue C-D dyes using diamond electrode. *Electrocatalysis*, 3, 1-12.
- [43] Mousset, E., Pechaud, Y., Oturan, N., Oturan, M. A. (2019). Charge transfer/mass transport competition in advanced hybrid electrocatalytic wastewater treatment: Development of a new current efficiency relation. *Applied catalysis B: Environmental*, 240, 102-111.
- [44] Scialdone, O., Galia, A., Guarisco, C., La Mantia, S. (2012). Abatement of 1, 1, 2, 2-tetrachloroethane in water by reduction at silver cathode and oxidation at boron doped diamond anode in micro reactors. *Chemical engineering journal*, 189, 229-236.
- [45] Mousset, E., Wang, Z., Olvera-Vargas, H., Lefebvre, O. (2018). Advanced electrocatalytic pre-treatment to improve the biodegradability of real wastewater from the electronics industry—a detailed investigation study. *Journal of hazardous materials*, 360, 552-559.
- [46] Raghu, S., Lee, C. W., Chellammal, S., Palanichamy, S. and Basha, C. A. (2009). Evaluation of electrochemical oxidation techniques for degradation of dye effluents – A comparative approach. *Journal of hazardous materials*, 171(1-3), 748-754.
- [47] Ammar, S., Oturan, M. A., Labiadh, L., Guersalli, A., Abdelhedi, R., Oturan, N., Brillas, E. (2015). Degradation of tyrosol by a novel electro-Fenton process using pyrite as heterogeneous source of iron catalyst. *Water research*, 74, 77-87.
- [48] Bae, S., Kim, D., Lee, W. (2013). Degradation of diclofenac by pyrite catalyzed Fenton oxidation. *Applied catalysis B: Environmental*, 134, 93-102.
- [49] Che, H., Bae, S., Lee, W. (2011). Degradation of trichloroethylene by Fenton reaction in pyrite 510 suspension. *Journal of hazardous materials*, 185, 1355-61.
- [50] Oturan, N., Brillas, E., Oturan, M. A. (2012). Unprecedented total mineralization of atrazine and cyanuric acid by anodic oxidation and electro-Fenton with a boron-doped diamond anode. *Environmental chemistry letters*, 10(2), 165-170.